

Wavevector analysis of the jellium exchange-correlation surface energy in the random-phase approximation: detailed support for nonempirical density functionals

J. M. Pitarke^{1,2}, Lucian A. Constantin³, and John P. Perdew³

¹*Materia Kondentsatuaren Fisika Saila, Zientzi Fakultatea, Euskal Herriko Unibertsitatea
644 Posta kutxatila, E-48080 Bilbo, Basque Country*

²*Donostia International Physics Center (DIPC) and Unidad Física Materiales CSIC-UPV/EHU,
Manuel de Lardizabal Pasealekua, E-20018 Donostia, Basque Country*

³*Department of Physics and Quantum Theory Group, Tulane University, New Orleans, LA 70118
(Dated: March 23, 2022)*

We report the first three-dimensional wavevector analysis of the jellium exchange-correlation (xc) surface energy in the random-phase approximation (RPA). The RPA accurately describes long-range xc effects which are challenging for semi-local approximations, since it includes the universal small-wavevector behavior derived by Langreth and Perdew. We use these rigorous RPA calculations for jellium slabs to test RPA versions of nonempirical semi-local density-functional approximations for the xc energy. The local spin density approximation (LSDA) displays cancelling errors in the small and intermediate wavevector regions. The PBE GGA improves the analysis for intermediate wavevectors, but remains too low for small wavevectors (implying too-low jellium xc surface energies). The nonempirical meta-generalized gradient approximation of Tao, Perdew, Staroverov, and Scuseria (TPSS meta-GGA) gives a realistic wavevector analysis, even for small wavevectors or long-range effects. We also study the effects of slab thickness and of short-range corrections to RPA.

PACS numbers: 71.10.Ca, 71.15.Mb, 71.45.Gm

I. INTRODUCTION

Modern electronic-structure calculations for atoms, molecules, and solids usually rely upon Kohn-Sham (KS) density-functional theory (DFT),^{1,2} in which only $E_{xc}[n]$, the exchange-correlation (xc) energy as a functional of electron density, must be approximated. Semi-empirical approximations tend to be limited to systems that resemble those in the fitted data set (typically small molecules), but nonempirical ones are constructed to satisfy universal constraints and so should have a wider range of applicability.³ For example, it is expected that a good description of chemical reactions at a solid surface requires a good description of both the molecules and the surface.

Jellium is a simple model of a simple metal, in which the valence electrons are neutralized by a uniform positive background that extends up to a sharp planar surface. The apparent success of the simplest density functional, the local spin density approximation (LSDA), for the jellium surface energy⁴ motivated early interest in density functionals and in refinements of the LSDA such as the generalized gradient approximation (GGA).^{5,6}

It was therefore a matter of some concern when wavefunction-based Fermi HyperNetted-Chain (FHNC)⁷ and fixed-node Diffusion Monte Carlo (DMC)⁸ calculations for jellium slabs (and their extrapolation to infinite thickness) predicted surface energies considerably higher than those obtained in the LSDA. Indeed, DMC is usually a gold standard of accuracy. However, it encounters special difficulties for jellium slabs;⁹ furthermore, the large deviations between the available DMC and LSDA calculations have been attributed in part to

inconsistency between the energy of the inhomogeneous system and that of the corresponding homogeneous electron gas.^{10,11} Recent approaches^{10,11,12,13,14,15,16} have all suggested that the actual jellium surface energies are only a little higher than those obtained in the LSDA. The jellium surface-energy story is presented in full detail in Ref. 16.

In this paper, we perform a detailed analysis of exchange and correlation in jellium slabs, *exact* at the level of the random phase approximation (RPA), to show that the most refined nonempirical density functional, the meta-generalized gradient approximation of Tao, Perdew, Staroverov, and Scuseria (TPSS meta-GGA),¹⁷ can account even for the most long-ranged xc effects at a jellium surface. This is a considerable achievement for a semi-local functional that is inherently more reliable for short-ranged effects than for long-ranged ones. RPA is known to be correct at long range; because it has serious deficiencies at short-range and, therefore, cannot be compared to standard versions of the semi-local functionals, we use RPA versions of these functionals in this test.

In order to separate long-range and short-range xc effects, we look at the surface contribution to the spherically-averaged real-space xc hole, averaged over the electron density of the system, and its Fourier transform (wavevector analysis). Langreth and Perdew⁵ showed that the exact xc energy of an arbitrary inhomogeneous system can be obtained from a three-dimensional (3D) Fourier transform of the spherical average of the xc hole density, which is a function of a 3D wavevector \mathbf{k} . In the case of a plane-bounded electron gas, this wavevector-dependent spherical average is dominated at long wavelengths ($k \rightarrow 0$) by the zero-point energy-shift of the newly created surface collective oscillations (surface plas-

mons) and takes a simple analytical form. This known limit has been used to carry out a wavevector interpolation correction to LSDA,⁵ PBE-GGA,¹³ and TPSS-metaGGA¹⁶ xc surface energies. The wavevector interpolation corrections to these functionals were controlled^{13,16} by using the exact RPA values reported in Ref. 12, and led to a consistent set of predicted surface energies.¹⁶

In a DFT context, the RPA is based upon the time-dependent Hartree approximation for the density-response function but replacing the occupied and unoccupied single-particle Hartree orbitals and energies by the corresponding eigenfunctions and eigenvalues of the KS Hamiltonian of DFT.⁵ Hence, it describes the exchange energy and the long-range part of the correlation energy correctly. Essentially *exact* RPA surface energies were evaluated from single-particle LSDA orbitals and energies in Ref. 12. These calculations provide an accurate standard against which approximate density functionals (in their RPA versions) can be tested and normed. The RPA versions of LSD and GGA were reported in Refs. 18 and 19, respectively. Because RPA is not self-correlation-free, the GGA for RPA correlation is its own meta-GGA. The RPA version of the nonempirical TPSS meta-GGA was investigated in Ref. 16.

Unless stated otherwise, atomic units are used throughout, i.e., $e^2 = \hbar = m_e = 1$.

II. THEORETICAL FRAMEWORK

The exact xc energy, $E_{xc}[n]$, of an arbitrary inhomogeneous system of density $n(\mathbf{r})$ can be obtained from the spherical average $\bar{n}_{xc}(\mathbf{r}, u)$ of the coupling-constant averaged xc hole density $\bar{n}_{xc}(\mathbf{r}, \mathbf{r}')$ at \mathbf{r}' around an electron at \mathbf{r} , as follows^{5,16}

$$E_{xc}[n] = \int d\mathbf{r} n(\mathbf{r}) \varepsilon_{xc}[n](\mathbf{r}), \quad (1)$$

where $\varepsilon[n](\mathbf{r})$ represents the xc energy per particle at point \mathbf{r} :

$$\varepsilon_{xc}[n](\mathbf{r}) = 4 \int_0^\infty dk \int_0^\infty du u^2 \frac{\sin ku}{ku} \bar{n}_{xc}(\mathbf{r}, u), \quad (2)$$

with

$$\bar{n}_{xc}(\mathbf{r}, u) = \frac{1}{4\pi} \int d\Omega \bar{n}_{xc}(\mathbf{r}, \mathbf{r}'), \quad (3)$$

$d\Omega$ being a differential solid angle around the direction of $\mathbf{u} = \mathbf{r}' - \mathbf{r}$.

The xc surface energy, σ_{xc} , is obtained by subtracting from the xc energy $E_{xc}[n]$ of a semi-infinite electron system the corresponding energy $E_{xc}^{\text{unif}}(n)$ of a uniform electron gas. In a jellium model, in which the electron system is translationally invariant in the plane of the surface, and assuming the surface to be normal to the z -axis, one finds

$$\sigma_{xc} = \int_0^\infty d\left(\frac{k}{2k_F}\right) \gamma_{xc}(k), \quad (4)$$

where²⁰

$$\gamma_{xc}(k) = 2 \frac{k_F}{\pi} \int_{-\infty}^{+\infty} dz n(z) b_{xc}(k, z), \quad (5)$$

with $k_F = (3\pi^2\bar{n})^{1/3}$, \bar{n} being the background density, and

$$b_{xc}(k, z) = 4\pi \int_0^\infty du u^2 \frac{\sin ku}{ku} [\bar{n}_{xc}(z, u) - \bar{n}_{xc}^{\text{unif}}(u)]. \quad (6)$$

Alternatively, one can introduce Eq. (3) into Eq. (6) to find:

$$b_{xc}(k, z) = \frac{1}{2} \int_{-k}^{+k} \frac{dk_z}{k} \int_{-\infty}^{+\infty} dz' e^{ik_z(z-z')} \times \bar{n}_{xc}(k_{\parallel}; z, z') - \bar{n}_{xc}^{\text{unif}}(k), \quad (7)$$

with $k_{\parallel} = \sqrt{k^2 - k_z^2}$, and $\bar{n}_{xc}(k_{\parallel}; z, z')$ and $\bar{n}_{xc}^{\text{unif}}(k)$ representing Fourier transforms of the coupling-constant averaged xc hole densities $\bar{n}_{xc}(\mathbf{r}, \mathbf{r}')$ and $\bar{n}_{xc}^{\text{unif}}(\mathbf{r}, \mathbf{r}')$, respectively. At long wavelengths ($k \rightarrow 0$), one finds the exact limit⁵

$$\gamma_{xc}(k) = \frac{k_F}{4\pi} \left(\omega_s - \frac{1}{2} \omega_p \right) k, \quad (8)$$

which only depends on the bulk- and surface-plasmon energies $\omega_p = (4\pi\bar{n})^{1/2}$ and $\omega_s = \omega_p/\sqrt{2}$, and does not depend, therefore, on the electron-density profile at the surface.

The spherical average $\bar{n}_{xc}(z, u)$ entering Eq. (6) can be obtained within local or semi-local density-functional approximations (such as LSDA, PBE GGA, and TPSS meta-GGA) from models^{16,19,21,22} that require knowledge of the xc hole density $\bar{n}_{xc}^{\text{unif}}(u)$ of a uniform electron gas. Alternatively, rigorous calculations of $\bar{n}_{xc}^{\text{unif}}(k)$ and the fully nonlocal $\bar{n}_{xc}(k_{\parallel}; z, z')$ entering Eq. (7) can be carried out from knowledge of the λ -dependent density-response functions $\chi_{\text{unif}}^\lambda(k, \omega)$ and $\chi^\lambda(k_{\parallel}; \omega; z, z')$, respectively, defined by adiabatically switching on the e-e interaction via the coupling constant λ and by adding, at the same time, an external potential so as to maintain the true ($\lambda = 1$) ground-state density in the presence of the modified e-e interaction.^{23,24} By using the fluctuation-dissipation theorem,^{25,26} one finds:

$$\bar{n}_{xc}^{\text{unif}}(k) = \frac{1}{\bar{n}} \left[-\frac{1}{\pi} \int_0^1 d\lambda \int_0^\infty d\omega \chi_{\text{unif}}^\lambda(k, i\omega) - \bar{n} \right] \quad (9)$$

and

$$\bar{n}_{xc}(k_{\parallel}; z, z') = -\frac{1}{\pi n(z)} \int_0^1 d\lambda \int_0^\infty d\omega \chi^\lambda(k_{\parallel}, i\omega; z, z') - \delta(z - z'). \quad (10)$$

With the aim of testing the performance of local and semi-local density-functional approximations for the xc surface energy, we compare these (local and semi-local)

calculations [obtained from Eq. (6)] to their fully non-local counterparts [obtained from Eq. (7) with the aid of Eqs. (9) and (10)] at the same level of approximation, which we choose to be the RPA. On the one hand, we evaluate $\gamma_{xc}(k)$ from RPA versions (LSDA-RPA, PBE-RPA, and TPSS-RPA) of the local (or semi-local) $\bar{n}_{xc}(z, u)$ entering Eq. (6) based on the RPA xc hole density $\bar{n}_{xc}^{\text{unif}}(u)$ of a uniform electron gas. On the other hand, we evaluate $\gamma_{xc}(k)$ from a fully nonlocal version (exact-RPA) of $\bar{n}_{xc}(k_{\parallel}; z, z')$ entering Eq. (7) based [by using Eq. (10)] on the RPA density-response function $\chi^{\lambda}(k_{\parallel}, \omega; z, z')$.

III. RESULTS

In the calculations presented below, we have considered a jellium slab of background thickness $a = 2.23 \lambda_F$, λ_F being the Fermi wavelength ($\lambda_F = 2\pi/k_F$), and background density $\bar{n} = [(4\pi/3)r_s^3]^{-1}$ with $r_s = 2.07$. This slab corresponds to about four atomic layers of Al(100).

For the LSDA-RPA calculations, we have obtained the RPA xc hole density $\bar{n}_{xc}^{\text{unif}}(u)$ of a uniform electron gas either from Eq. (9) or from a non-oscillatory parametrization.²⁷ For the PBE-RPA and TPSS-RPA calculations, we have always used a non-oscillatory parametrization of the RPA xc hole density $\bar{n}_{xc}^{\text{unif}}(u)$.²⁷

For the evaluation of the fully nonlocal (exact-RPA) $\gamma_{xc}(k)$ of Eq. (5), we follow the method described in Ref. 12. We first assume that $n(z)$ vanishes at a distance z_0 from either jellium edge,²⁸ and we expand the single-particle wave functions $\phi_l(z)$ and the density-response function $\chi^{\lambda}(k_{\parallel}, \omega; z, z')$ in sine and double-cosine Fourier representations, respectively. We then perform the integrals over the coordinates z and z' analytically, and we find an explicit expression for $\gamma_{xc}(k)$ [see Eqs. (A1)-(A5) of the Appendix] in terms of the single-particle energies ε_l and the Fourier coefficients b_{ls} and $\chi_{mn}(k_{\parallel}, \omega)$ of the single-particle wave functions $\phi_l(z)$ and the density-response function $\chi^{\lambda}(k_{\parallel}, \omega; z, z')$, respectively.²⁹ We have taken all the single-particle wave functions $\phi_l(z)$ and energies ε_l to be the LDA eigenfunctions and eigenvalues of the KS Hamiltonian of DFT, as obtained by using the Perdew-Wang parametrization¹⁸ of the Ceperley-Alder xc energy of the homogeneous electron gas.³⁰ For the jellium slab with $r_s = 2.07$ and $a = 2.23\lambda_F$ considered here, the *exact* RPA xc surface energy is found to be $\sigma_{xc} = 3091 \text{ erg/cm}^2$, not far from the corresponding RPA xc surface energy of a semi-infinite jellium which is known to be $\sigma_{xc} = 3064 \text{ erg/cm}^2$.¹⁰

In Figs. 1 and 2 we have plotted (solid lines) the exact-exchange contribution to $\gamma_{xc}(k)$, i.e., $\gamma_x(k)$, which we have obtained from Eqs. (A1)-(A5) with the quantities $\chi_{\text{unif}}^{\lambda}(k, \omega)$ and $\chi_{mn}^{\lambda}(k_{\parallel}, \omega)$ replaced by their noninteracting counterparts $\chi_{\text{unif}}^0(k, \omega)$ and $\chi_{mn}^0(k_{\parallel}, \omega)$, respectively. Also plotted in these figures are the LSDA, PBE, and TPSS calculations of $\gamma_x(k)$ that we have obtained by replacing the xc hole densities $\bar{n}_{xc}(z, u)$ and $\bar{n}_{xc}^{\text{unif}}(u)$ enter-

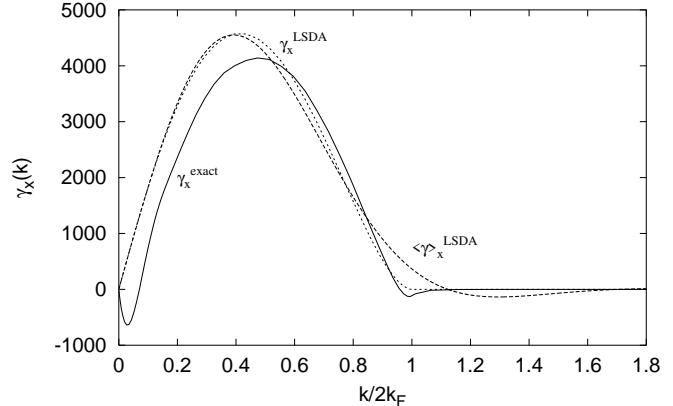


FIG. 1: Wavevector analysis $\gamma_x(k)$, versus $k/2k_F$, of the exchange surface energy of a jellium slab of thickness $a = 2.23\lambda_F$ and $r_s = 2.07$. Solid and dashed lines represent *exact* and LSDA calculations, respectively. The LSDA calculation has been performed either from the actual exchange hole density $n_x^{\text{unif}}(u)$ of a uniform electron gas, which we have obtained from Eq. (9) with $\chi_{\text{unif}}^{\lambda}(k, \omega)$ replaced by $\chi_{\text{unif}}^0(k, \omega)$, (γ_x^{LSDA}) or from the non-oscillatory parametrization of $n_x^{\text{unif}}(u)$ reported in Ref. 22 ($\langle \gamma \rangle_x^{\text{LSDA}}$). The area under each curve represents the exchange surface energy: $\sigma_x^{\text{LSDA}} = 2699 \text{ erg/cm}^2$ and $\sigma_x^{\text{exact}} = 2348 \text{ erg/cm}^2$. (1 hartree/bohr² = $1.557 \times 10^6 \text{ erg/cm}^2$.)

ing Eq. (6) by their corresponding exchange-only counterparts (dashed lines).

The LSDA $\gamma_x(k)$ represented in Fig. 1 has been obtained by using both the actual exchange hole density $n_x^{\text{unif}}(u)$ of a uniform electron gas [dashed curve labeled γ_x^{LSDA}], which we have obtained from Eq. (9) with $\chi_{\text{unif}}^{\lambda}(k, \omega)$ replaced by $\chi_{\text{unif}}^0(k, \omega)$, and the non-oscillatory exchange hole density $n_x^{\text{unif}}(u)$ reported in Ref. 22 [dashed curve labeled $\langle \gamma \rangle_x^{\text{LSDA}}$]. $\gamma_x^{\text{LSDA}}(k)$ and $\langle \gamma \rangle_x^{\text{LSDA}}(k)$ yield, by construction of the non-oscillatory exchange hole density $n_x^{\text{unif}}(u)$, the same exchange surface energy σ_x ; they are also almost identical in a wide range of low wavevectors, but $\langle \gamma \rangle_x^{\text{LSDA}}(k)$ is considerably less accurate near $k = 2k_F$ where the exact $\gamma_x(k)$ has a kink. This kink is realistic for jellium-like systems, but not for atoms and molecules.

The PBE and TPSS $\gamma_x(k)$ represented in Fig. 2 have both been obtained by using the non-oscillatory exchange hole density $n_x^{\text{unif}}(u)$ reported in Ref. 22, which yields a wrong behavior of $\gamma_x(k)$ at large wavevectors. Nevertheless, both the actual exchange hole density $n_x^{\text{unif}}(u)$ of a uniform electron gas (not used in these calculations) and the corresponding non-oscillatory exchange hole density would yield the same exchange surface energy σ_x , by construction, as occurs in the LSDA.

Figs. 1 and 2 show that while the LSDA $\gamma_x(k)$ considerably overestimates the exact $\gamma_x(k)$ at low wavevectors (see Fig. 1), leading to an exchange surface energy σ_x that is too large, the PBE and TPSS $\gamma_x(k)$ are close to the ex-

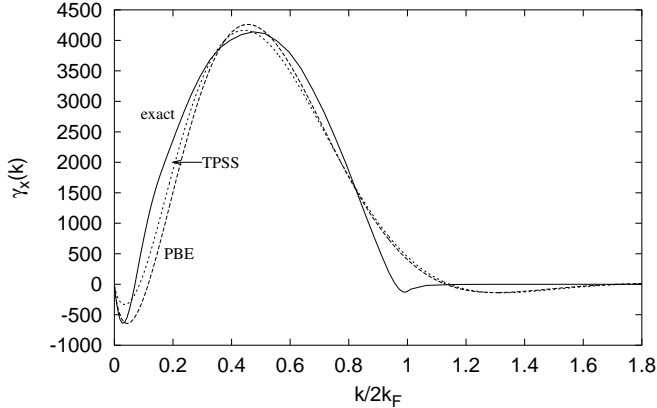


FIG. 2: Wavevector analysis $\gamma_x(k)$, versus $k/2k_F$, of the exchange surface energy of a jellium slab of thickness $a = 2.23\lambda_F$ and $r_s = 2.07$. Solid and dashed lines represent *exact* and semi-local (PBE and TPSS) calculations, respectively. The semi-local PBE and TPSS calculations have been performed from the non-oscillatory parametrization of $n_x^{\text{unif}}(u)$ reported in Ref. 22. The area under each curve represents the exchange surface energy: $\sigma_x^{\text{PBE}} = 2155 \text{ erg/cm}^2$, $\sigma_x^{\text{TPSS}} = 2247 \text{ erg/cm}^2$, and $\sigma_x^{\text{exact}} = 2348 \text{ erg/cm}^2$.

act $\gamma_x(k)$ (see Fig. 2). We note that the peaks of $\gamma_x^{\text{PBE}}(k)$ and $\gamma_x^{\text{TPSS}}(k)$ are close to the exact one, a fact which was used in the construction of the TPSS exchange hole,¹⁶ and that at larger wavevectors $\gamma_x^{\text{PBE}}(k)$ and $\gamma_x^{\text{TPSS}}(k)$ nearly coincide, as expected; at lower wavevectors, however, the TPSS meta-GGA differs from the PBE GGA, leading to a wavevector-dependent $\gamma_x(k)$ that is closer to the exact behavior.

We have also carried out calculations of the exact $\gamma_x(k)$ for increasing values of the background thickness a , and we have found that (i) $\gamma_x(k)$ is only sensitive to the size of the system at wavevectors below the minimum that is present in the solid lines of Figs. 1 and 2, and (ii) as $k \rightarrow 0$ the wavevector-dependent $\gamma_x(k)$ approaches in the semi-infinite limit the profile-independent negative value ($\gamma_x = -1.50 \times 10^4 / r_s^3 \text{ erg/cm}^2$) reported in Refs. 5 and 31.

Figures 3 and 4 exhibit the results that we have obtained for the RPA $\gamma_{xc}(k)$ from Eqs. (A1)-(A5) (solid lines) and within the LSDA-RPA, PBE-RPA, and TPSS-RPA (dashed lines). As in the case of the exchange-only contributions represented in Figs. 1 and 2, the LSDA $\gamma_{xc}(k)$ represented in Fig. 3 has been obtained by using both the actual RPA xc hole density $\bar{n}_{xc}^{\text{unif}}(u)$ [dashed line labeled $\gamma_{xc}^{\text{LSDA-RPA}}$], which we have obtained from Eq. (9), and a non-oscillatory xc hole density $\bar{n}_{xc}^{\text{unif}}(u)$ [dashed line labeled $\langle \gamma \rangle_{xc}^{\text{LSDA-RPA}}$]; the PBE and TPSS $\gamma_{xc}(k)$ represented in Fig. 4 have both been obtained by using a non-oscillatory xc hole density $\bar{n}_{xc}^{\text{unif}}(u)$.

Figure 3 shows that at short wavelengths with $k > 2k_F$ the quantities $\gamma_{xc}^{\text{LSDA-RPA}}(k)$ (dashed line) and $\gamma_{xc}^{\text{exact-RPA}}(k)$ (solid line) nearly coincide, as

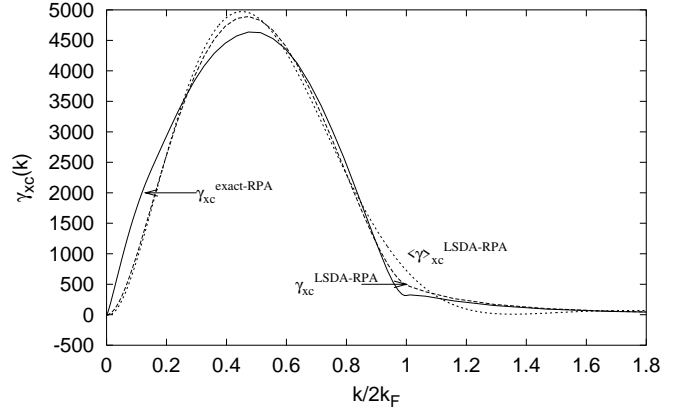


FIG. 3: Wavevector analysis $\gamma_{xc}(k)$, versus $k/2k_F$, of the RPA xc surface energy of a jellium slab of thickness $a = 2.23\lambda_F$ and $r_s = 2.07$. Solid and dashed lines represent exact-RPA and LSDA-RPA calculations, respectively. The LSDA calculation has been performed either from the actual RPA xc hole density of Eq. (9) ($\gamma_{xc}^{\text{LSDA-RPA}}$) or from a non-oscillatory parametrization of $\bar{n}_{xc}^{\text{unif}}(u)$ ($\langle \gamma \rangle_{xc}^{\text{LSDA}}$).²⁷ The area under each curve represents the RPA xc surface energy: $\sigma_{xc}^{\text{LSDA-RPA}} = 3034 \text{ erg/cm}^2$ and $\sigma_{xc}^{\text{exact-RPA}} = 3091 \text{ erg/cm}^2$.

expected.^{5,32,33} The LSDA, however, considerably underestimates $\gamma_{xc}(k)$ at low wavevectors. This is *partially* compensated by an LSDA $\gamma_{xc}(k)$ that at intermediate wavevectors (around the peak of $\gamma_{xc}(k)$) is too large. Figure 4 shows that the PBE GGA improves $\gamma_{xc}(k)$ at intermediate wavevectors more than at low wavevectors, thereby yielding a xc surface energy that is even smaller than in the LSDA. From a different perspective,³⁴ the too-small PBE surface energy arises from a too-large gradient coefficient for exchange, but this is repaired by the TPSS meta-GGA which uses the proper gradient coefficient. Indeed, Fig. 4 clearly shows that the TPSS meta-GGA brings improvements over the corresponding PBE GGA at both intermediate and small wavevectors, thus leading to a wavevector-dependent $\gamma_{xc}^{\text{TPSS-RPA}}(k)$ that is very close to $\gamma_{xc}^{\text{exact-RPA}}(k)$ (solid line) and to an xc surface energy σ_{xc} that is only slightly lower than its exact RPA counterpart.³⁵ We have obtained similar results (not displayed here) for $r_s = 3$, and we have found that the errors introduced by the use of nonempirical semi-local density-functional approximations slightly increase with r_s as expected from the analysis of Ref. 16.

Also represented in Fig. 4 (by a dotted line) is the universal (density-profile independent) low-wavevector limit of Eq. (8). The TPSS-RPA $\gamma_{xc}(k)$ has the virtue that not only is it very close to its exact-RPA counterpart in the whole range of low and intermediate wavevectors, but it imitates the exact low-wavevector limit of Eq. (8) as well. That this limit is also reproduced by the exact-RPA $\gamma_{xc}(k)$ of a semi-infinite electron system is shown in Fig. 5, where we have plotted calculations of this quantity for increasing values of the background thickness a , from

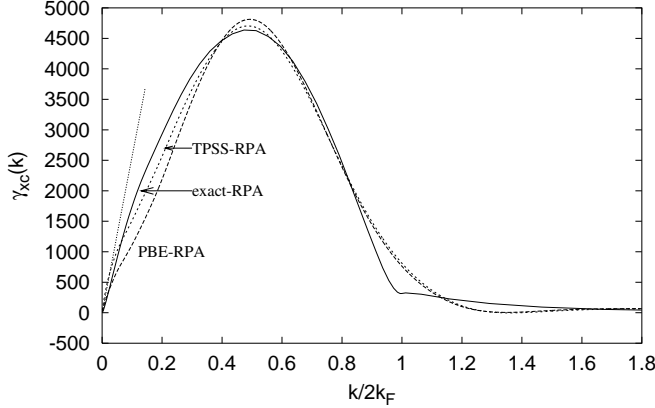


FIG. 4: Wavevector analysis $\gamma_{xc}(k)$, $k/2k_F$, of the RPA xc surface energy of a jellium slab of thickness $a = 2.23\lambda_F$ and $r_s = 2.07$. Solid and dashed lines represent exact-RPA and semilocal-RPA (PBE-RPA and TPSS-RPA) calculations, respectively. The semilocal PBE-RPA and TPSS-RPA calculations have been performed from a non-oscillatory parametrization of $\bar{n}_{xc}^{\text{unif}}(u)$.²⁷ The area under each curve represents the RPA xc surface energy: $\sigma_{xc}^{\text{PBE-RPA}} = 2959 \text{ erg/cm}^2$, $\sigma_{xc}^{\text{TPSS-RPA}} = 3052 \text{ erg/cm}^2$, and $\sigma_{xc}^{\text{exact-RPA}} = 3091 \text{ erg/cm}^2$. The straight dotted line represents the universal low-wavevector limit of Eq. (8).

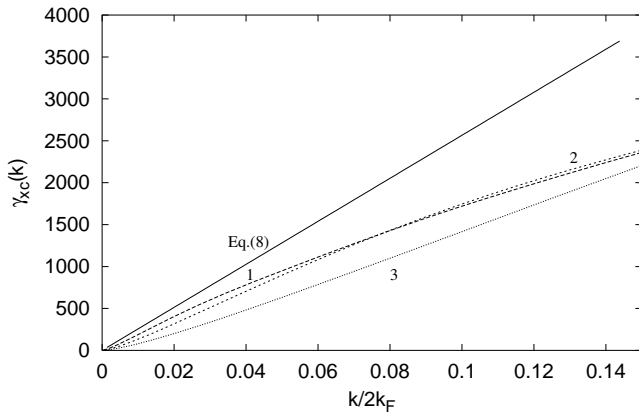


FIG. 5: Wavevector analysis $\gamma_{xc}(k)$, versus $k/2k_F$, of the exact RPA xc surface energy of jellium slabs of $r_s = 2.07$ and various values of the background thickness: $a = 8.23\lambda_F$ ('1'), $a = 2.23\lambda_F$ ('2'), and $a = 0.56\lambda_F$ ('3'). The straight solid line represents the universal low-wavevector limit of Eq. (8), which corresponds to a plane-bonded semi-infinite system ($a \rightarrow \infty$).

$a = 0.56\lambda_F$ to $a = 8.23\lambda_F$. Furthermore, Fig. 6 shows that $\gamma_{xc}(k)$ is only sensitive to the background thickness at very low wavevectors.

Finally, in order to investigate the impact of short-range corrections to the RPA $\gamma_{xc}(k)$, we have plotted in Fig. 7 the correlation contribution to $\gamma_{xc}(k)$, i.e., $\gamma_c(k)$, as obtained in the RPA (LSDA-RPA, TPSS-RPA,

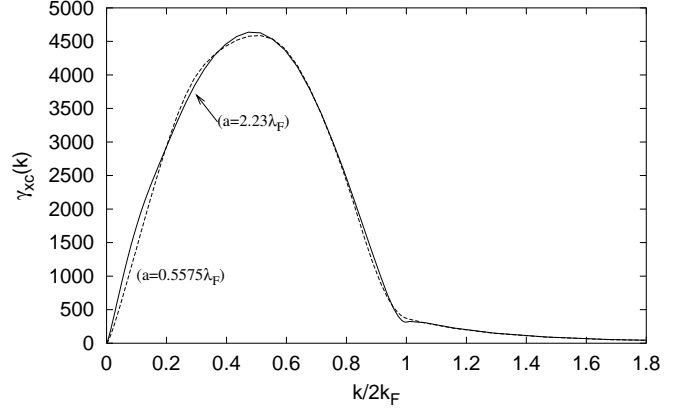


FIG. 6: Wavevector analysis $\gamma_{xc}(k)$, versus $k/2k_F$, of the exact RPA xc surface energy of jellium slabs of $r_s = 2.07$ and two values of the background thickness: $a = 2.23\lambda_F$ (solid line) and $a = 0.56\lambda_F$ (dashed line). The area under each curve represents the exact RPA xc surface energy $\sigma_{xc}^{\text{exact-RPA}}$: 3091 erg/cm^2 and 3043 erg/cm^2 , for $a = 2.23\lambda_F$ and $a = 0.56\lambda_F$, respectively.

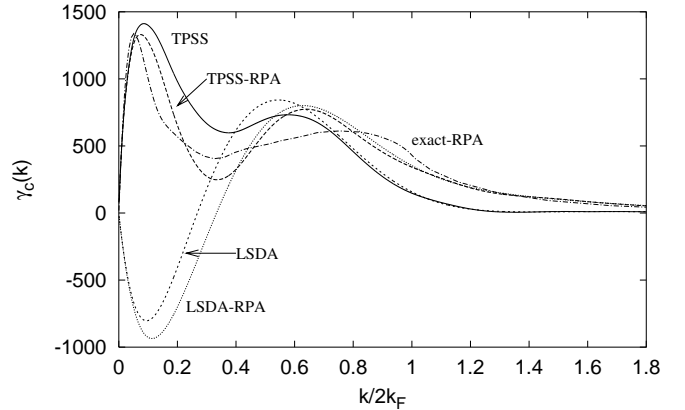


FIG. 7: Wavevector analysis $\gamma_c(k)$, versus $k/2k_F$, of the correlation surface energy of a jellium slab of thickness $a = 2.23\lambda_F$ and $r_s = 2.07$. Dotted, long-dashed, and dashed-dotted lines represent LSDA-RPA, TPSS-RPA, and exact-RPA calculations, respectively. Short-dashed and solid lines represent standard versions of the LSDA and the semi-local TPSS, as obtained from an accurate (beyond RPA) non-oscillatory parametrization of the correlation hole density $\bar{n}_c^{\text{unif}}(u)$ of a uniform electron gas.²¹ The area under each curve represents the correlation surface energy: $\sigma_c^{\text{LSDA-RPA}} = 336 \text{ erg/cm}^2$, $\sigma_c^{\text{TPSS-RPA}} = 804 \text{ erg/cm}^2$, $\sigma_c^{\text{exact-RPA}} = 743 \text{ erg/cm}^2$, $\sigma_c^{\text{LSDA}} = 290 \text{ erg/cm}^2$, and $\sigma_c^{\text{TPSS}} = 756 \text{ erg/cm}^2$.

and exact-RPA) and also in standard versions of local and semi-local density-functionals (LSDA and TPSS) that use an accurate (beyond RPA) non-oscillatory parametrization of the correlation hole density $\bar{n}_c^{\text{unif}}(u)$ of a uniform electron gas.²¹ We observe that in the long-wavelength limit ($k \rightarrow 0$), where both LSDA-RPA and

standard LSDA exhibit serious deficiencies, both TPSS-RPA and the more accurate *standard* TPSS coincide with the exact-RPA. At shorter wavelengths, the *standard* TPSS predicts a substantial correction to its TPSS-RPA and exact-RPA counterparts, which is first positive and then negative and leads, therefore, to a persistent cancellation of short-range correlation effects beyond the RPA similar to the cancellation that was reported in Ref. 10 in the framework of time-dependent density-functional theory and a two-dimensional wavevector analysis of the correlation surface energy.

IV. CONCLUSIONS

We have reported the first 3D wavevector analysis of the jellium xc surface energy in the RPA, and we have used this fully nonlocal (essentially exact) RPA calculation to test RPA versions of nonempirical semi-local density-functional approximations for the xc energy. We have tested the first three-rungs of the Jacob's ladder classification of nonempirical density functionals:³⁶ LSDA, PBE GGA, and TPSS meta-GGA.

We have found that while the LSDA displays cancelling errors in the small and intermediate wavevector regions and the PBE GGA improves the analysis for intermediate wavevectors while remaining too low for small wavevectors (implying two-low xc surface energies), the TPSS meta-GGA yields a realistic wavevector analysis even for small wavevectors or long-range effects. We have also demonstrated numerically the correctness of the LSDA at large wavevectors^{5,32,33} (where LSD-RPA, TPSS-RPA, and the exact-RPA coincide, as shown in Fig. 7) and the universal low-wavevector behavior derived by Langreth and Perdew,⁵ which is nicely reproduced by the TPSS meta-GGA.

We have carried out fully nonlocal RPA calculations for increasing values of the background thickness, and we have found that the 3D wavevector analysis of the xc surface energy is remarkably insensitive to the slab thickness except at very long wavelengths ($k \rightarrow 0$) where decreasing the slab thickness reduces the universal slope that is dictated by the presence of bulk and surface collective oscillations.

Finally, we have found that the TPSS wavevector analysis of the correlation surface energy, as obtained from an accurate (beyond RPA) non-oscillatory parametrization of the xc hole density of a uniform electron gas, provides both the exact short- k limit, where LDA fails badly, and the exact large- k limit, where RPA is wrong. Hence, our calculations support the conclusion that the TPSS meta-GGA xc density functional accurately describes the jellium surface, including not only short-range but also

long-range effects.

Acknowledgments

J.M.P. acknowledges partial support by the University of the Basque Country, the Basque Unibertsitate eta Ikerketa Saila, the Spanish Ministerio de Educación y Ciencia, and the EC 6th framework Network of Excellence NANOQUANTA (Grant No. NMP4-CT-2004-500198). L.A.C. and J.P.P. acknowledge the support of the U.S. National Science Foundation under grant DMR-0501588.

APPENDIX A

Here we give an explicit expression for the wavevector-dependent contribution $\gamma_{xc}(k)$ to the xc surface energy σ_{xc} of a jellium slab of background density \bar{n} and thickness a , in terms of the single-particle energies ϵ_l and the Fourier coefficients b_{ls} and χ_{mn}^λ of the single-particle wave functions $\phi_l(z)$ and the density-response function $\chi_\lambda(k_\parallel; z, z')$, respectively.²⁹ From Eqs. (5), (7), (9), and (10) and performing the integrals over the coordinates z and z' analytically, we find:

$$\gamma_{xc}(k) = \frac{k_F}{\pi} \left[\int_0^k \frac{dk_z}{k} \sum_{m=0}^{\infty} \sum_{n=0}^{\infty} \alpha_{mn}(k_z) \beta_{mn}(k_\parallel) - \bar{n} a \bar{n}_{xc}^{\text{unif}}(k) \right], \quad (\text{A1})$$

where

$$\alpha_{mn}(k_z) = 2k_z^2 \frac{1 - (-1)^m \cos(k_z d)}{[k_z^2 - (m\pi/d)^2][k_z^2 - (n\pi/d)^2]} \quad (\text{A2})$$

and¹²

$$\beta_{mn}(k_\parallel) = -\frac{1}{\pi} \int_0^1 d\lambda \int_0^\infty d\omega \chi_{mn}^\lambda(k_\parallel, i\omega) - \frac{\mu_m \mu_n}{\pi d^2} \sum_{l=1}^{l_M} (E_F - \epsilon_l) \sum_{l'=1}^{\infty} G_{ll'}^m G_{ll'}^n, \quad (\text{A3})$$

with $d = a + 2z_0$,

$$\mu_m = \begin{cases} 1, & \text{for } m = 0, \\ 2, & \text{for } m \geq 1, \end{cases} \quad (\text{A4})$$

and

$$G_{ll'}^m = \frac{1}{2} \sum_{s=1}^{\infty} \sum_{s'=1}^{\infty} b_{ls} b_{l's'} (\delta_{m,s-s'} + \delta_{m,s'-s} - \delta_{m,s+s'}). \quad (\text{A5})$$

¹ W. Kohn and L.J. Sham, Phys. Rev. **140**, A1133 (1965).

² R. M. Dreizler and E. K. U. Gross, *Density-Functional*

- Theory. An Approach to the Quantum Many-Body Problem*, Springer, 1990.
- ³ S. Kurth, J.P. Perdew and P. Blaha, *Int. J. Quantum Chem.* **75**, 889 (1999).
 - ⁴ N.D. Lang and W. Kohn, *Phys. Rev. B* **1**, 4555 (1970).
 - ⁵ D.C. Langreth and J.P. Perdew, *Phys. Rev. B* **15**, 2884 (1977); **21**, 5469 (1980); **26**, 2810 (1982).
 - ⁶ J.P. Perdew, K. Burke and M. Ernzerhof, *Phys. Rev. Lett.* **77**, 3865 (1996), and references therein.
 - ⁷ E. Krotscheck, W. Kohn, and G.-X. Qian, *Phys. Rev. B* **32**, 5693 (1985); E. Krotscheck and W. Kohn, *Phys. Rev. Lett.* **57**, 862 (1986).
 - ⁸ P.H. Acioli and D.M. Ceperley, *Phys. Rev. B* **54**, 17199 (1996).
 - ⁹ W.M.C. Foulkes and B. Wood, private communication.
 - ¹⁰ J.M. Pitarke and J.P. Perdew, *Phys. Rev. B* **67**, 045101 (2003).
 - ¹¹ J.M. Pitarke, *Phys. Rev. B* **70**, 087401 (2004).
 - ¹² J.M. Pitarke and A.G. Eguiluz, *Phys. Rev. B* **57**, 6329 (1998); **63**, 045116 (2001).
 - ¹³ Z. Yan, J.P. Perdew, S. Kurth, C. Fiolhais, and L. Almeida, *Phys. Rev. B* **61**, 2595 (2000).
 - ¹⁴ L.M. Almeida, J.P. Perdew, and C. Fiolhais, *Phys. Rev. B* **66**, 075115 (2002).
 - ¹⁵ J. Jung, P. Garcia-González, J. F. Dobson, and R.W. Godby, *Phys. Rev. B* **70**, 205107 (2004).
 - ¹⁶ L.A. Constantin, J.P. Perdew and J. Tao, *Phys. Rev. B*, to appear.
 - ¹⁷ J. Tao, J.P. Perdew, V.N. Staroverov, and G.E. Scuseria, *Phys. Rev. Lett.* **91**, 146401 (2003).
 - ¹⁸ J.P. Perdew and Y. Wang, *Phys. Rev. B* **45**, 13244 (1992).
 - ¹⁹ Z. Yan, J.P. Perdew, and S. Kurth, *Phys. Rev. B* **61**, 16430 (2000).
 - ²⁰ We are considering here a plane-bounded semi-infinite electron system. In the case of a jellium slab, the right-hand side of Eq. (5) should be divided by a factor of 2.
 - ²¹ J. P. Perdew and Y. Wang, *Phys. Rev. B* **46**, 12947 (1992).
 - ²² M. Ernzerhof and J.P. Perdew, *J. Chem. Phys.* **109**, 3313 (1998).
 - ²³ D.C. Langreth and J.P. Perdew, *Solid State Comm.* **17**, 1425 (1975).
 - ²⁴ O. Gunnarsson and B. I. Lundqvist, *Phys. Rev. B* **13**, 4274 (1976).
 - ²⁵ H.B. Callen and T.R. Welton, *Phys. Rev.* **83**, 34 (1951).
 - ²⁶ D. Pines and P. Nozieres, *The Theory of Quantum Liquids*, Addison-Wesley, 1989.
 - ²⁷ For the exchange contribution to $\bar{n}_{xc}^{unif}(u)$ we have used the non-oscillatory parametrization reported in Ref. 22. For the RPA correlation contribution to $\bar{n}_{xc}^{unif}(u)$ we have used the non-oscillatory parametrization reported in Ref. 19 within the framework of Ref. 21.
 - ²⁸ z_0 is chosen sufficiently large for the physical results to be insensitive to the precise value employed.
 - ²⁹ A. G. Eguiluz, *Phys. Rev. B* **31**, 3303 (1985).
 - ³⁰ D. M. Ceperley and B. J. Alder, *Phys. Rev. Lett.* **45**, 566 (1980).
 - ³¹ M. Rasolt and D. J. W. Geldart, *Phys. Rev. B* **25**, 5133 (1982).
 - ³² K. Burke and J.P. Perdew, *Int. J. of Quantum Chem.* **56**, 199 (1995).
 - ³³ K. Burke, J.P. Perdew and D.C. Langreth, *Phys. Rev. Lett.* **73**, 1283 (1994).
 - ³⁴ J.P. Perdew, L.A. Constantin, E. Sagvolden, and K. Burke, submitted for publication.
 - ³⁵ TPSS-RPA xc surface energies of a semi-infinite jellium are indeed very close to (and usually slightly lower than) their exact RPA counterparts, as shown in Table I of Ref. 16.
 - ³⁶ J.P. Perdew and K. Schmidt, in *Density Functional Theory and Its Application to Materials*, edited by V.E. Van Doren, K. Van Alsenoy, and P. Geerlings (American Institute of Physics, Melville, NY, 2001).